Magnetic behavior of the semimagnetic semiconductor cadmium manganese arsenide ((Cd1-xMnx)3As2)

Magnetic behavior of the semimagnetic semiconductor $(Cd_{1-x}Mn_x)_3As_2$

C. J. M. Denissen, H. Nishihara,* J. C. van Gool, and W. J. M. de Jonge
Department of Physics, Eindhoven University of Technology, Eindhoven, The Netherlands
(Received 9 September 1985)

The magnetization, susceptibility, and specific heat of the semimagnetic semiconductor $(Cd_{1-x}Mn_x)_3As_2$ have been measured in the temperature range 0.5 K $< T <$ 300 K and in magnetic fields up to 25 T for $x < 18\%$. A transition to a spin-glass state is observed at low temperatures. The results indicate that a relatively strong antiferromagnetic (AF) nearest-neighbor interaction J_0 is present together with an AF long-range interaction of the type J_1/R^3 or J_1/R^4. The magnetic moment on the Mn sites turns out to be about 4.4 Bohr magnetons and no deviation from a random distribution of the magnetic ions is observed. Based on these observations we calculated the thermodynamic properties with the extended nearest-neighbor pair correlation approximation. It appears that this approximation gives a good description of C_m, M, and χ simultaneously with $J_0/k_B = -30$ K and $J_1/k_B = -20/R^4$ K (R in units of the nearest-neighbor distance). Possible application of the model to other semimagnetic semiconductors and the possible origin of the exchange mechanism in $(Cd_{1-x}Mn_x)_3As_2$ are discussed.

I. INTRODUCTION

$(Cd_{1-x}Mn_x)_3As_2$, or CMA, can be considered as a solid solution of the zero-gap semiconductors Cd_3As_2 and Mn_3As_2. In an earlier publication[1] it has been shown by the present authors that, for low Mn concentrations ($x < 0.2$), the behavior of this system resembles that of a novel class of materials which have been termed semimagnetic semiconductors (SMSC), which includes compounds like CdMnTe, CdMnSe, HgMnSe, HgMnTe, PbMnTe, etc. The properties of these materials have been extensively reviewed recently by Brandt and Moshchalkov.[2]

An essential feature of the SMSC's is the interaction between the localized magnetic moments and the mobile band electrons, which gives rise to rather anomalous effects in the free-carrier behavior as well as in the magnetic properties. In this paper we will restrict ourselves to the last item. For additional information on the band structure, optical and transport properties we refer to the publications of Blom *et al.*[3]

In the study of the magnetic properties of SMSC's, two types of distinct, although related, problems can be distinguished. The first problem concerns the physical interactions inducing the commonly observed spin-glass behavior at low temperatures, and the second problem deals with the description of the thermodynamic properties in terms of interactions between the magnetic ions and the statistical distribution of them. In the majority of SMSC studied so far, a spin-glass transition is observed at low temperatures. Since it appeared in the first experimental reports[4,5] that such a spin-glass transition was restricted to magnetic-ion concentrations above the percolation limit of the host lattice, it was concluded that this transition was induced by short-range interactions between nearest-neighbor magnetic ions causing frustration effects. In our first report on CMA, however, we noted that in this system the freezing transition also exists for vanishingly small impurity contents. Quite recently, similar observations were reported for several other SMSC's HgMnTe,[6] PbMnTe,[7] CdMnTe,[8] and CdMnSe.[9] This fact indicates that a rather long-range interaction between the magnetic ions must be responsible for the freezing transition. However, unlike the more canonical type of metallic spin-glasses such as Cu (Mn), the Ruderman-Kittel-Kasuya-Yosida (RKKY) oscillatory type of exchange can be ruled out in this case because of the relatively low concentration of carriers ($N_e = 10^{18}$ cm^{-3}). Although several other exchange mechanisms have been proposed, the physical background of the interaction is still rather obscure.

On the other hand, the description of the behavior of SMSC's in the paramagnetic state is hampered by the fact that, so far, no consistent set of parameters has been obtained which explain all the relevant data. For two representative examples, CdMnTe and HgMnTe, exchange parameters ranging over more than one order of magnitude have been reported, together with rather contradictory statements about the statistical distribution of the magnetic impurities.[2] According to recent publications of Shapira *et al.*[10] at least part of this confusion might be traced back to the use of oversimplified models which have been applied to a limited set of data. However, an effort to effectively reconcile these contradictory viewpoints has, to our knowledge, not been undertaken yet.

In view of the present state of the art on SMSC's, we thought it worthwhile to study the properties of CMA in some detail. As quoted above, earlier observations showed that the properties of CMA resemble those of a SMSC in many ways. In this paper we will report the susceptibility, magnetization and specific heat results in a wide temperature and field range and we will try to interpret all these data simultaneously on the basis of one model incorporating a nearest-neighbor as well as a long-range interaction in a random array.

II. STRUCTURE AND SAMPLE PREPARATION

The CMA samples were grown by a modified Bridgman method at a temperature of 780—800 °C, in carbon-coated quartz ampoules containing stoichiometric amounts of the pure elements. The composition and homogeneity of all the samples were characterized by electron-micropobe measurements, x-ray diffraction, and chemical analysis. Single-phase samples were always obtained for $x < 0.1$. At larger concentrations, sometimes small amounts of ferromagnetic MnAs could be detected. The measured concentration x varied slightly over the ingot and thus over the samples, which had typical dimensions of $1 \times 1 \times 1$ cm^3. The relative accuracy of x is therefore estimated as $\pm 10\%$. Zdanowicz *et al.*[11] have described the preparation and structure of CMA in more detail.

The crystal structure of Cd_3As_2 has been reported by Steigman and Goodyear.[12] The Cd atoms, which are partially substituted by Mn in CMA, are situated on the corners of a simple cubic cell with systematic vacancies on one diagonal.

III. EXPERIMENTAL RESULTS

A. Low-temperature ac susceptibility

The ac susceptibility was measured with a conventional mutual inductance bridge operating in the region 90 Hz $< \nu <$ 900 Hz. The results for CMA for various x are shown in Fig. 1. The results below 1 K were obtained in a dilution refrigerator for which no adequate absolute calibration of χ was available, which may result in some systematic deviations of the data at low temperatures. Nevertheless pronounced cusps in $\chi(T)$ are observed, which, as we will see later on, are absent in the specific heat. The susceptibility is rather insensitive to the frequency in the range $\nu < 900$ Hz. Moreover, small fields up to 0.01 T only slightly smooth the cusps. No appreciable hysteresis was observed. Interpreting the cusp as a transition to a spin-glass state, the resulting phase boundary $T_f(x)-x$ is shown in Fig. 2 in the range $2\% < x < 18\%$. It appears that $T_f \to 0$ when $x \to 0$. T_f varies approximately with $x^{4/3}$, although a simple linear dependence is not quite excluded. From this experimental observation one may conjecture that the interactions inducing this spin-glass transition are long ranged, since otherwise no freezing should have been observed for $x < x_c$, the percolation limit which amounts to 33% in this case. Moreover, scaling arguments[13,14] relate the specific concentration dependence of T_f, $T_f \approx x$ or $T_f \approx x^{4/3}$, to a long-range exchange of the type J_1/R^3 or J_1/R^4, respectively, where R is the distance between the magnetic ions. Similar observations have been reported recently for HgMnTe,[6,15] CdMnTe,[8] and CdMnSe[9].

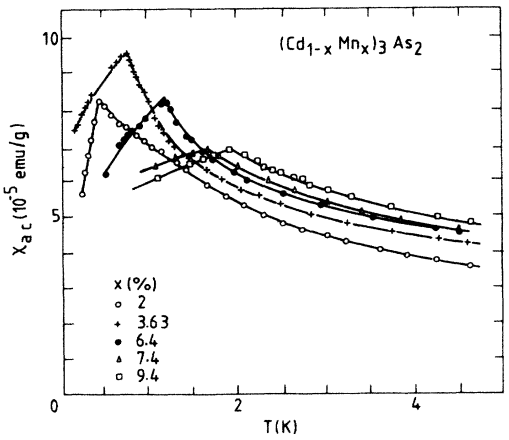

FIG. 1. Low-temperature ac susceptibility of CMA.

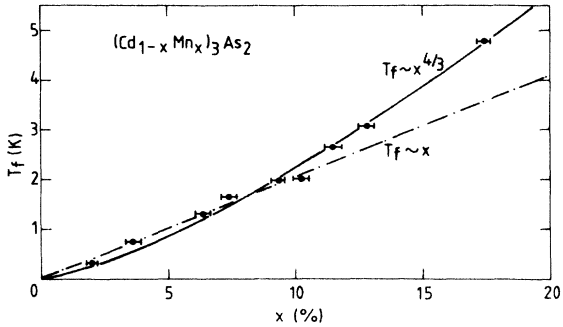

FIG. 2. Freezing temperature as function of x for CMA. Dashed-dotted curve and solid curve represent the prediction for T_f based on scaling with $J \approx R^{-3}$ and $J \approx R^{-4}$, respectively.

B. Specific heat

Specific-heat data were obtained with a conventional adiabatic heat pulse calorimeter in the range 0.3 K $< T <$ 20 K. The magnetic contribution C_m to the specific heat was obtained by subtraction of the (scaled) lattice contribution of pure Cd_3As_2 and the nuclear hyperfine contribution of the Mn ions.

The results for zero external field are shown in Fig. 3(a). As quoted above, no anomaly was observed at the temperature T_f, indicated by arrows in the figure. The overall contribution shows a broad maximum, typically for an ensemble of interacting spins, where the temperature of the maximum is a measure for the magnitude of the average interaction energy. Note that the maximum shifts systematically to higher temperature (from 0.5 K to 5 K) as the concentration increases from 1% to 10%. This behavior indicates that the average interaction increases more or less proportional with concentration, which is consistent with the notion of a long-range interaction. Further indications for the long-range character of the interactions can be obtained from scaling invariance. It has been shown by Souletie and by Tholence and Tournier[13] that when the interaction is a function of the distance, a simple correspondence between C_m, x, and T can be established in a diluted alloy. For an interaction of the type J_1/R^3, this would result in a universal function when C_m/x is plotted against T/x. The experimental results are shown in Fig. 3(b). Indeed a fair degree of data

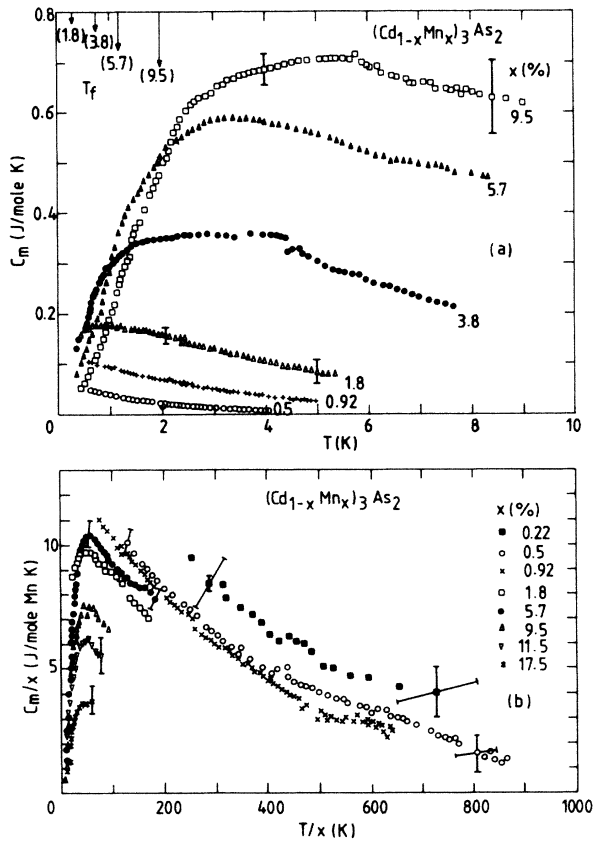

FIG. 3. (a) Magnetic specific heat of CMA. The arrows indicate the freezing temperature T_f for the corresponding concentrations. (b) Scaled magnetic specific heat Cm/x as function of the scaled temperature T/x. This scaling is based on $J \approx R^{-3}$.

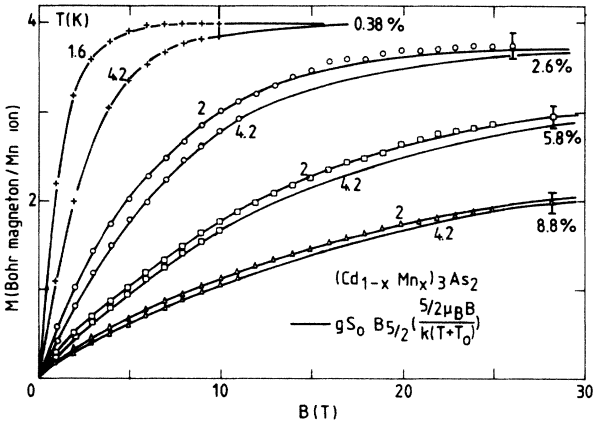

FIG. 4. High-field magnetization M of CMA for selected concentrations. The solid lines represent fits with the phenomenological Brillouin function.

reduction can be observed. In the next paragraph we will present evidence that strong antiferromagnetic interaction will lead to pairing of statistically nearest neighbor Mn ions. At the present low-temperature range these pairs will not contribute to C_m. Modification of x to x_{eff}, which excludes the nearest-neighbor paired Mn ions, indeed considerably improves the data reduction. On the other hand, the data reduction is worse when a long-range interaction of the type J_1/R^4 is assumed. In neither case, however, it is perfect and in our opinion it yields no pertinent evidence about the specific dependence of the interaction on distance.

C. Magnetization

Magnetization measurements were performed in the field range up to 25 T and the temperature range 2 K $< T <$ 4.2 K. In the low-field range ($B < 6$ T) a Foner magnetometer was employed. The high-field measurements were performed with a pulsed field flux method. Some representative results are shown in Fig. 4.

From a comparison of the overall behavior as compared with that of an ideal paramagnetic gas it can be concluded that the average interaction must be antiferromagnetic. Furthermore, an increase of the concentration yields an obvious increase of the average interaction. Saturation in the present field range is achieved for the concentrations lower than 3%.

Gaj *et al.*[16] have introduced a phenomenlogical Brillouin function in order to describe the magnetization of SMSC's. In this approach the magnetization per Mn ion can be written as

$$M = g\mu_B S_0 B_{5/2}\left[\frac{5/2 g\mu_B B}{k_B T_{\text{eff}}}\right]. \quad (1)$$

The saturation magnetization per Mn ion $g\mu_B S_0$ and the effective temperature $T_{\text{eff}} = T + T_0$ are considered as adjustable parameters. For the sake of comparison we also fitted our magnetization results of CMA with this Brillouin function as shown in Fig. 4. The obtained gS_0 and T_0 are given in Table I.

The saturation moments per ion are plotted in Fig. 5 against x, supplemented with extrapolated results based on fits of the data to a phenomenological Brillioun function for higher concentrations. Two features of this figure are noteworthy. First, these results show that, in the limit of vanishingly small concentrations of magnetic ions, the saturation moment per ion $g\mu_B S_0$ approaches the value of 4.2±0.2 Bohr magnetons instead of the value of 5 Bohr magnetons anticipated from the conjecture that

TABLE I. Results of fitting with the phenomenological Brillouin function [Eq. (1)].

x (%)	gS_0	T_0 (K)
0.23	4.2	
0.38	4.0	0.9
0.55	4.3	
0.72	4.0	
2.6	3.8	10.8
5.8	3.3	22
8.8	2.5	31

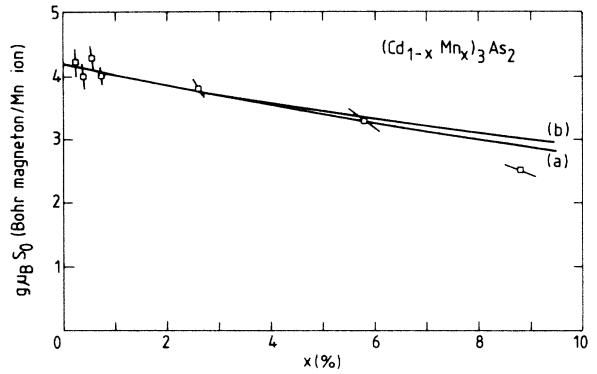

FIG. 5. Saturation magnetization per Mn ion, $g\mu_B S_0$, as function of the concentration x for CMA. Curve a represents the contribution of the statistical fraction of the singles to the saturation. Curve b includes also the contribution of $\frac{1}{3}$ of the statistical fraction of open triples.

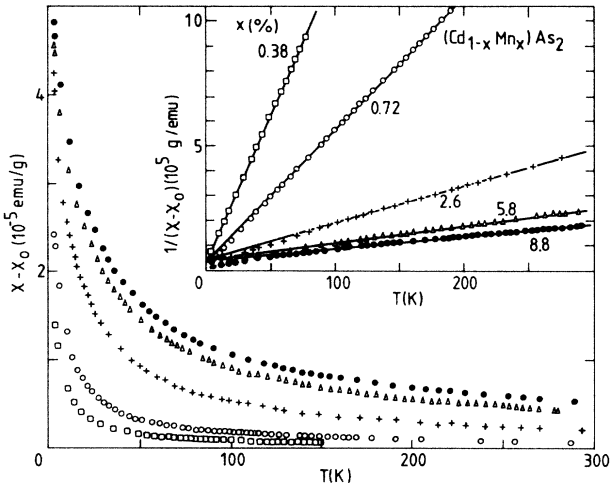

FIG. 6. High-temperature susceptibility of CMA. The inset shows the inverse susceptibility, in which the solid lines represent the limiting high-temperature Curie-Weiss behavior according to Eq. (2). In both figures the same symbols are used for corresponding x.

the ground state of the localized Mn^{2+} moments would be an S state. Although such a reduction of the free-ion moment cannot be excluded *a priori* in a semimetallic surrounding, it has not been observed in other SMSC's. In metallic spin glasses, however, it is a usual phenomenon. Susceptibility results which will be discussed below support this conclusion. Second, another feature worth mentioning is the apparent reduction of the measured saturation value when the concentration increases. Besides the data points we also plotted in Fig. 5 the theoretical moment under the assumption that nearest-neighbor pairs do not contribute in this field range, for instance because they are strongly coupled antiferromagnetically and the ground state is a singlet state. The fractions of singles and triples have been obtained from random statistics. Comparison of the actual data with this prediction shows a remarkably good agreement, although one has to recall that the data at high x are based on extrapolated results. Recently, Aggarwal *et al.* and Shapira *et al.*[10] also observed such pairing in ZnMnSe and CdMnSe. In that case the interpretation was somewhat more direct, since they observed also a decoupling of the pairs in still higher fields. Since we do not observe any decoupling in fields up to 28 T, the antiferromagnetic nearest-neighbor coupling in CMA amounts to at least 40 K, or alternatively, $|J_0/k_B| > 20$ K.

D. High-temperature susceptibility

Susceptibility measurements were performed up to 300 K in a field of a few thousand oersted with a Faraday balance. The ac susceptibility results measured up to 80 K agree reasonably with these results. The data, corrected for a diamagnetic contribution of Cd_3As_2, which was determined separately as -3.10^{-7} emu/g, are shown in Fig. 6. At sufficiently high temperature all the data appear to follow a Curie-Weiss behavior given by

$$\chi-\chi_0=C/(T-\Theta)\ . \tag{2}$$

The slope of the $1/(\chi-\chi_0)$-T plot is determined by the factor

$$\frac{3xNg^2\mu_B^2 S(S+1)}{3k_B M}\ ,$$

where M is the molecular weight and N is Avogadro's number. The resulting values for $g[S(S+1)]^{1/2}$ and gS (assuming $g=2$) are given in Table II. Again, as was already anticipated from the high-field magnetization data, the moment per Mn ion ($4.7\pm0.2\mu_B$) appears to be smaller than the free-ion value ($5\mu_B$). For all concentrations x, the Curie-Weiss temperature Θ is negative [antiferromagnetic (AF)] and is roughly proportional to x as plotted in Fig. 7.

We would like to stress at this point that Θ obtained from this high-temperature data contains all the interactions (nearest-neighbor as well as long-range), in contrast to the other data reported above (at low-temperature and relatively small-field) where as we saw before, strong antiferromagnetic nearest interactions may eliminate the contribution of even numbered statistical clusters. If we adopt, for the moment, a model in which the localized

TABLE II. Results obtained from the slope of the inverse susceptibility versus T, at high temperature (see also inset of Fig. 6).

x (%)	$g[S(S+1)]^{1/2}$	gS ($g=2$)
0.38	5.4	4.5
0.72	5.8	4.9
2.6	5.8	4.9
5.8	5.7	4.8
8.8	5.4	4.5

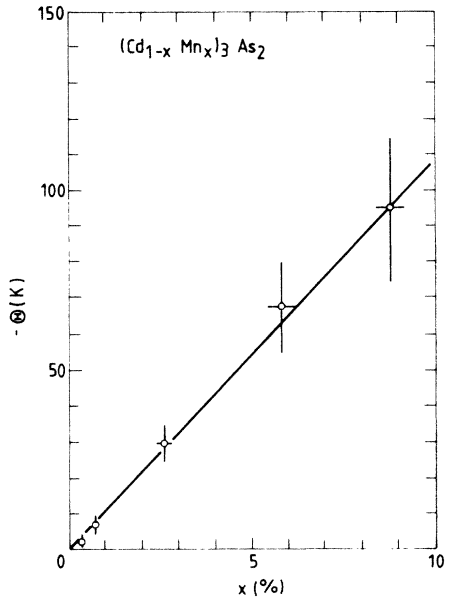

FIG. 7. Curie-Weiss temperature as function of x. The solid line represents $\Theta = -1080x$.

magnetic moments are subjected to a nearest-neighbor exchange J_0 and a long-range interaction of the type $J = J_1/R^4$, high-temperature series expansion (HTSE) gives

$$\Theta = \frac{2S(S+1)x}{3k_B}\left[N_1 J_0 + \sum_{j=2}^{\infty} \frac{J_1 N_j}{R_j^4}\right], \tag{3}$$

which for CMA results in (assuming $S=2$)

$$\Theta = \frac{x}{k_B}(16J_0 + 31.1J_1), \tag{4}$$

where N_j is the number of neighbors at distance R_j (R_j expressed in units of the nearest-neighbor Mn distance).

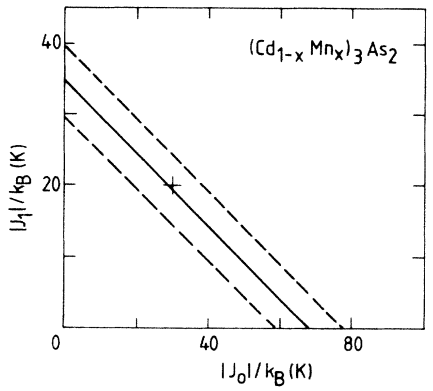

FIG. 8. Representation of the relation $(16|J_0| + 31.1|J_1|)/k_B = 1080$, obtained from Eq. (4) and the slope of $\Theta - x$. The dashed lines represent the relation for the two extreme slopes of $\Theta - x$, which can be obtained from Fig. 7. The cross marks J_0 and J_1, used in extended nearest-neighbor pair correlation approximation (ENNPA).

Comparing this expression with the experimentally observed $\Theta = -1080x$ in Fig. 7 yields a relation between the strength of the two interaction parameters J_0 and J_1 as plotted in Fig. 8.

We would like to note also that the linearity of Θ versus x is not a result of the specific R^4 dependence of the long-range interactions. Only the prefactors in Eq. (4) will alter when another radial dependence is used. However for J_1/R^n, $n \leq 3$ the sum in Eq. (3) is not convergent and the prefactor of J_1 can not be found unless damping effects or oscillations of the long-range interaction are taken into account. The linearity basically rests on the assumption that the magnetic ions are randomly distributed in the lattice. The observed proportionality between Θ and x therefore appears to support this conjecture.

IV. INTERPRETATION

A first inspection of the experimental zero-field specific heat, magnetization, and susceptibility data has shown so far that these results can be, at least qualitatively, understood on the basis of the following assumptions:

(i) A relatively strong AF nearest-neighbor interaction J_0.

(ii) An AF long-range interaction of the type J_1/R^n where n is 3 or 4.

(iii) A random array.

(iv) $gS \simeq 4.4$, the average between magnetization and susceptibility results (or since we would like to work with "real" spin values, $g = 2.2$ and $S = 2$).

In the following, we will now try to calculate the relevant thermodynamic properties of such a magnetic array and compare the results with the actual data in order to verify whether it is possible to obtain a consistent description of the various data based on the above mentioned assumptions.

The inclusion of a long-ranged interaction yields a rather complex Hamiltonian. In the earlier approximations used for SMSC's,[5] use has been made of a model in which the array has been build up from singles, pairs, triples, etc., with only a nearest-neighbor interaction. However, this model is not applicable in this case since the long-range interaction implies that all moments are coupled. This is particularly important for the zero-field specific heat where, in contrast to the earlier approaches, the singles (in the sense that they have no magnetic nearest neighbors but interact with neighbors further apart) probably form the major contribution to the total magnetic specific heat at low concentrations. Discarding this contribution almost inevitably leads to uprating of the numbers of clusters above their statistical weight corresponding to a random distribution in order to fit the experimental data.

Following Ref. 17 we have calculated the thermodynamic properties by means of the so-called pair-correlation model. The basic assumption on which this method rests can be stated as the partition function of a macroscopic system with a fixed random distribution of spins may be factorized into contributions of pairs of

spins. Thus each spin is considered to belong to one pair formed with its nearest magnetic neighbor which may be located anywhere. We have extended this model by taking into account one kind of triple correlation: we corrected for the spins which have two magnetic neighbors at the same distance. This model can be considered as a version of the model employed by Morgownik and Mydosh,[18] who obtained excellent results with this approach in the description of some metallic spin-glasses.

The sites of the crystalline host structure are arranged in shells at distances $\{R_\nu,\ \nu=1,2,3,\cdots\}$ around the reference site; the νth shell contains N_ν sites. Using

$$n_\nu=\sum_1^\nu N_\nu \quad \text{for} \quad \nu>0 \text{ and } n_0=0\ , \tag{5}$$

the probability of finding the nearest spin in the νth shell, for the random case is

$$P_\nu(x)=(1-x)^{n_{\nu-1}}-(1-x)^{n_\nu}\ . \tag{6}$$

The probability for finding two neighbors in the same shell (spin in a triple) is

$$P_\nu^T(x)=\frac{N_\nu(N_\nu-1)}{2}x^2(1-x)^{n_\nu-2}\ . \tag{7}$$

The probability for a spin in a pair is taken as

$$P_\nu^P(x)=P_\nu(x)-P_\nu^T(x)\ . \tag{8}$$

The Hamiltonians for a pair and a triple are given by

$$H_\nu^P=-2J_\nu\mathbf{S}_i\cdot\mathbf{S}_\nu-g\mu_B(S_i^z+S_\nu^z)B^z\ , \tag{9}$$

$$H_\nu^T=-2J_\nu\mathbf{S}_i\cdot\mathbf{S}_{\nu,1}-2J_\nu\mathbf{S}_i\cdot\mathbf{S}_{\nu,2} -g\mu_B(S_i^z+S_{\nu,1}^z+S_{\nu,2}^z)B^z\ , \tag{10}$$

where $J_\nu=J_0$ for $\nu=1$ and $J_\nu=J_1/R_\nu^n$ for $\nu>1$. R_ν is in units of the nearest-neighbor distance.

The total free energy and other thermodynamic functions like the specific heat, magnetization, and susceptibility can be calculated from the pair and triple contribution:

$$F=\sum_{\nu=1}^{\infty}P_\nu^P(x)F_\nu^P/2+P_\nu^T(x)F_\nu^T/3\ , \tag{11}$$

$$C_m=\sum_{\nu=1}^{\infty}P_\nu^P(x)C_{m,\nu}^P/2+P_\nu^T(x)C_{m,\nu}^T/3,\ \cdots\ . \tag{12}$$

The calculations were performed numerically. Therefore we were forced to use "real" spin values and we chose $g=2.2$ and $S=2$, resulting in $gS\simeq 4.4$ as indicated by magnetization and susceptibility experiments. The summation over the shells (ν) in Eqs. (11) and (12) is carried out up to shell $\nu=\bar{\nu}$ for which $\sum_{\nu=1}^{\bar{\nu}}P_\nu^P(x)+P_\nu^T(x)\geq 99.5$. Figure 9 shows an actual distribution for $x=2.6\%$, together with the occupation of triples in each shell which have been taken into account. The value of $\bar{\nu}$ was taken as 17 in this case. For higher concentrations of x, a smaller $\bar{\nu}$ was sufficient, for lower concentrations $\bar{\nu}$ was increased.

In the calculations, J_0 and J_1 were treated as adjustable parameters. The results of such a calculation are shown in Figs. 10, 11, and 12. Since on the whole the overall agreement for J_1/R^3 is somewhat worse than J_1/R^4 and the phase diagram T_f-x also gives a stronger indication

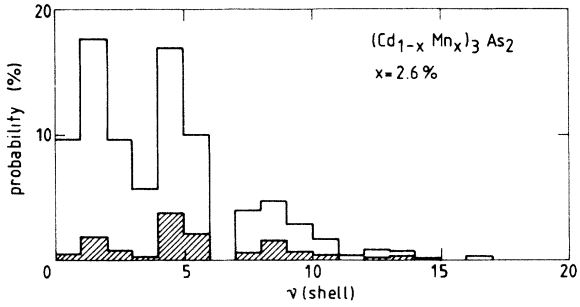

FIG. 9. Probability of finding a neighbor in shell ν [pair, Eq. (8)] represented by the blank histogram and probability of finding two neighbors in shell ν [triple, Eq. (7)] represented by the shaded histogram.

for J_1/R^4 we chose to present the latter. We would like to emphasize at this point that the theoretical curves shown in Figs. 10, 11, and 12 do not represent the best possible fit of each thermodynamical property separately. J_0 and J_1 were chosen such that the best overall agreement for all three experimental quantities is obtained. The most important feature is probably that these results show that it is in principle possible to explain the behavior of the specific heat, susceptibility and magnetization *simultaneously*, on the basis of the chosen set of assumptions.

Additionally we would like to make the following comments. As stated above, the magnitudes of the values of J_0 and J_1 have been obtained from the best overall agreement of all the accessible data. This may not be completely correct. The extended nearest-neighbor pair correlation approximation (ENNPA) used in the calculation, is probably a worse approximation for higher concentrations, because the role of large clusters is not taken into account. In that light the agreement of the data with this

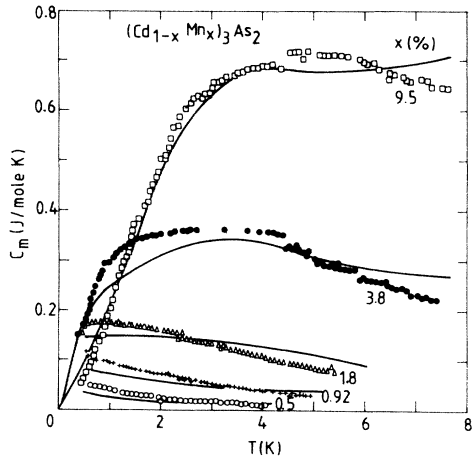

FIG. 10. Magnetic specific heat of CMA. The solid lines represent calculations with the approximation (ENNPA) as described in the text using $J_0/k_B=-30$ K and $J_1/k_B=-20/R^4$ K.

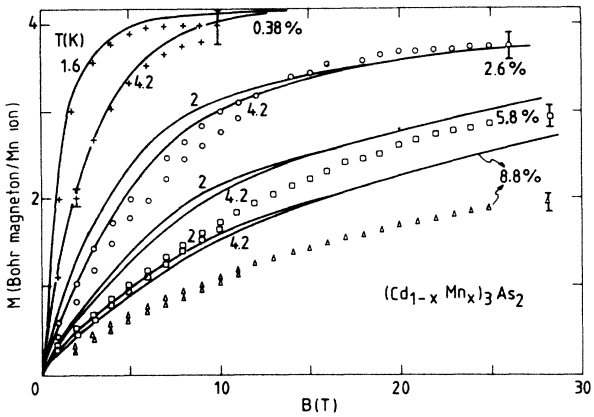

FIG. 11. High-field magnetization M of CMA. The solid lines represent calculations with the approximation (ENNPA), using $J_0/k_B = -30$ K and $J_1/k_B = -20/R^4$ K.

model at the highest percentages may be considered as fortuitous. If one only aims for a good agreement at low concentrations, the parameter value for $|J_1|$ tends to decrease somewhat. Second, it should be noted that the parameter values of J_0 and J_1 do not influence the results in a comparable way. In fact, the behavior of C_m is completely determined by J_1 in the present temperature range, since the direct contribution of nearest-neighbor pairs is negligible in the temperature range studied. The same is more or less valid for the magnetization, although of course the pairing of statistically nearest neighbors decreases the apparent saturation in the measured field range as we have shown before. Therefore J_0 is in fact only determined by the high-temperature susceptibility where J_1 as well as J_0 contribute [see Eqs. (3) and (4)].

For the Curie-Weiss temperature we obtained an exact result by HTSE [Eq. (4)]. Although the extended pair correlation model is an approximation, we checked whether Eq. (4) with J_0 and J_1 from the ENNPA agrees with the experimental $\Theta(x)$. The agreement is quite good, as is shown in Fig. 8.

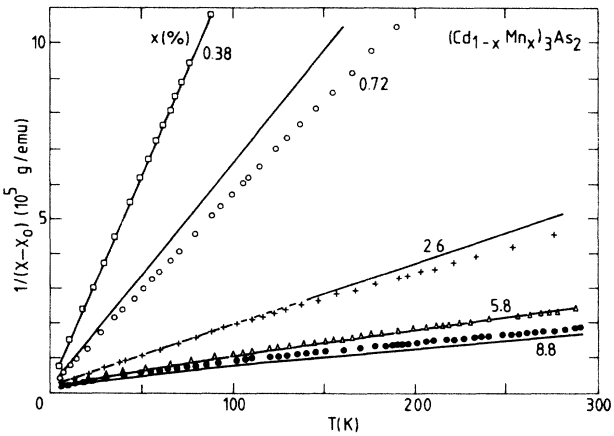

FIG. 12. Inverse high-temperature susceptibility of CMA. The solid lines represent calculations with the approximation (ENNPA), using $J_0/k_B = -30$ K and $J_1/k_B = -20/R^4$ K.

V. CONCLUDING REMARKS AND DISCUSSION

In the preceding paragraph we have given a model which describes the data on the specific heat, susceptibility, and magnetization simultaneously. The model contains nearest-neighbor and long-range antiferromagnetic exchange and assumes a random distribution of magnetic ions. Of course a number of questions remain to be answered. These questions relate to the origin of the reduction of the Mn spin S, the applicability of the pair correlation model for high concentrations and the consequences for the present interpretation. However, answering these questions requires further investigation which is currently underway. In the remainder of this paper we will focus on three issues; the applicability of our model to other SMSC's, the possible origin of the long-range interaction and the existence of the spin-glass phase.

As we quoted in the Introduction, one of our aims in the present investigation was to provide a model which simultaneously would explain the behavior of various thermodynamic quantities. One may therefore ask whether this model can also successfully be applied to comparable SMSC's. In order to investigate this point, we performed preliminary calculations of C_m and M for HgMnTe and compared these results with data reported by Nagata *et al.*[5] and by Dobrowolski *et al.*[19] So far, these data have been interpreted separately with cluster models and strongly modified statistical distributions. Since HgMnTe also displays a $T_f(x)$ for low x, which can be described with $T_f \approx x^{4/3}$, indicating a long-range contribution J_1/R^4, the present model may be applicable. As an illustration, Figs. 13 and 14 show preliminary results

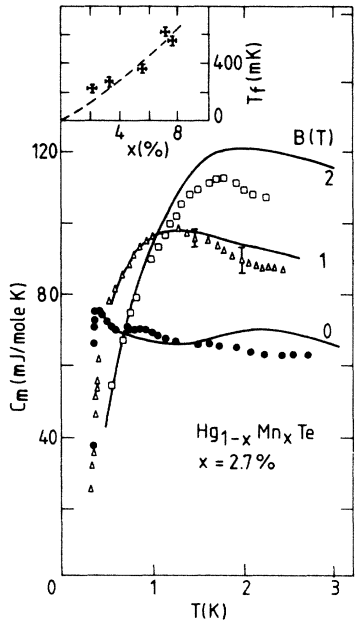

FIG. 13. Magnetic specific heat of $Hg_{1-x}Mn_xTe$ for $x = 2.7\%$. The solid lines represent calculations with the ENNPA, using $J_0/k = -4$ K, $J_1/k_B = -2.5/R^4$, $S = 2.5$, and $g = 2$. The inset shows T_f as a function of x. The dashed line yields $T_f \approx x^{4/3}$, indicating $J_1/k_B \approx R^{-4}$.

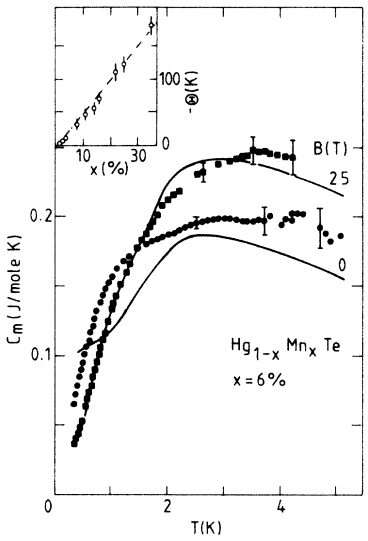

FIG. 14. Magnetic specific heat of $Hg_{1-x}Mn_xTe$ for $x=6\%$. The solid lines represent calculations with the ENNPA, using $J_0/k_B=-4$ K, $J_1/k_B=-2.5/R^4$ K, $S=2.5$, and $g=2$. In the inset, Θ as function of x is given. The dashed-dotted line yields the prediction of Eq. (3) using J_0/k_B and J_1/k_B as obtained from the ENNPA.

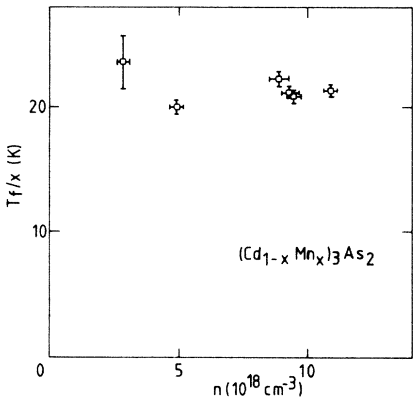

FIG. 15. T_f/x as a function of the electron concentration n for CMA.

for C_m based on some low-concentration data which were available to us. The calculations for the magnetization (not shown here) are in good agreement with the data. Moreover, the exchange parameters J_0 and J_1 used in this fit yield a Curie-Weiss temperature Θ [according to Eq. (3)] which agrees with the experimental high-temperature susceptibility (see inset Fig. 14). Judging from these results we are tempted to conclude that, at least for low concentrations, x, in this case a theoretical description of the data is also possible, assuming a nearest-neighbor exchange and long-range exchange of the type J_1/R^4. No deviation of random statistics is necessary. A more detailed comparison also comprising other SMSC's such as CdMnTe, is currently undertaken and will be published elsewhere.

In canonical metallic spin-glasses, the long-range interaction is commonly assumed to originate from the polarization of the free carriers. It can be expressed by the RKKY interaction which for a parabolical band can be written as[20]

$$J_{\mathrm{RKKY}}(R)\approx(A/R^4)[k_FR\cos(k_FR)-\sin(k_FR)]\ , \qquad (13)$$

where k_F is the Fermi wave vector and R is the distance between the ions. In CMA (and other SMSC's for that matter), the electron density is rather small resulting in $k_F=7.10^8$ m^{-1} with a nearest-neighbor distance $a_0=3.17\times10^{-10}$ m. Therefore the RKKY interaction cannot be approximated by a R^{-3} dependence since k_F is rather small. Instead Eq. (13) should read $J_{\mathrm{RKKY}}\approx A'n/R$, where n is the electron concentration. Moreover, for $R<10a_0$, the interaction according to Eq. (13) is ferromagnetic. It is clear that these predictions are not in agreement with our observations. To illustrate the specific n dependence, we prepared a series of CMA crystals with nearly constant Mn concentration but with somewhat varying electron concentration n. The electron concentration was varied by doping with traces of Cu or annealing in a Cd-rich environment. Figure 15 shows that no significant change in T_f could be detected in the range $3\times10^{18}<n<11\times10^{18}$ cm^{-3} in contrast with the RKKY prediction for J.

As an alternative, the interaction may be due to the polarization of the valence electrons (virtual interband interactions), as shown by Lewiner and Bastard,[21] which may be very effective in zero-gap semiconductors since the exponential damping factor of the Bloembergen-Rowland mechanism[22] becomes zero. If a positive gap ϵ_0 exists between the conduction and valence bands, the interaction is antiferromagnetic and can be written as[21,22]

$$J(R)\approx f(R)\exp(-k_0R)\ . \qquad (14)$$

$k_0=\hbar^{-1}(2m^*\epsilon_0)^{1/2}$, where m^* is the sum of the electron and hole masses.

For vanishing small gap ϵ_0 the exponential decay vanishes and the radial dependence is crucially determined by the specific dispersion of the valence and conduction bands. Lewiner *et al.*[21] calculated the interaction according this mechanism for two specific electronic band structures. For linear bands (which occur for instance at the zero-gap→semiconductor transition) a power-law behavior is obtained:

$$J(R)\approx R^{-n} \text{ with } 4<n<5\ . \qquad (15)$$

For parabolic bands they found[21]

$$J(R)\approx R^{-4}\ . \qquad (16)$$

It has been suggested that this mechanism is responsible for the long-range interactions in HgMnTe, CdMnTe, and CdMnSe,[8,9,15,21] although another mechanism has also been proposed.[23] The suggestion is based, among others, on the decrease of T_f with increasing band gap (as observed in quaternary alloys such as HgCdMnTe with a given Mn concentration).[15] Also the smaller T_f for the wide-gap compound CdMnTe as compared with the T_f of the narrow-gap compound HgMnTe can be qualitatively

understood with this mechanism.[8]

Whether this mechanism is also responsible for the interaction in CMA however, remains, to be seen. Similar to HgMnTe, $(Cd_{1-x}Mn_x)_3As_2$ is also a zero-gap semiconductor for low x. Extrapolation of Shubnikov–de Haas results for $x=0.01$ and $x=0.02$,[24] indicated a zero-gap→semiconductor transition at $x\simeq(6\pm1)\%$. The same effect occurs in $Hg_{1-x}Mn_xTe$ at $x\simeq7.5\%$.[6] In the T_f-x diagram of CMA no significant change in behavior is observed in this concentration range, while in HgMnTe an anomaly has been suggested.[6]

Moreover we have prepared quaternary alloys $(Cd_{1-y-x}Zn_yMn_x)_3As_2$. The substitution of Zn in Cd_3As_2 has been shown to increase the gap.[25] Comparing T_f in alloys with the same Mn concentration ($x=10\%$) but with different Zn concentration we found that T_f *increases* with Zn concentration. This is in marked disagreement with the expectation based on the Bloembergen-Rowland mechanism.

There is experimental evidence that rather-long-range superexchange interactions may be present in some compounds.[26] For the spinel $Fe_{1/2}Cu_{1/2}Rh_2S_4$, the spin structure can only be explained by taking into account distant-neighbor interactions involving exchange paths Fe-S-Rh-S-Fe and Fe-S-Rh-S-Rh-S-Fe. In Ref. 27 it is theoretically shown that superexchange due to the hybridization of the d states with the valence-band states can be long-range. For a parabolic band state this interaction is antiferromagnetic and given by

$$J(R)\approx(A/R^2)\exp(-k_0R)+(B/R)\exp(-k_0R)\ , \qquad (17)$$

where k_0 is the electron wave vector which governs the energy of the hybridized state. For small k_0 the above interaction is long-range. It has been suggested that superexchange contributes to the exchange in a semimagnetic semiconductor as $Pb_{1-x}Mn_xTe$,[28] although other mechanisms have been proposed.[7] Very recently it was shown by theoretical calculations that superexchange is dominant in CdMnTe.[23] Also various spectroscopic measurements yielded evidence on the presence of strong hybridization effects of the $3d$ states in CdMnTe.[29] Whether these effects, which can induce long-range superexchange, are present in CMA remains to be investigated. The reduction of the local moments compared to their purely ionic state, as observed in CMA, might be considered as an indication to that effect.

Finally we would like to comment on the existence of a spin-glass transition in semimagnetic semiconductors. To start with, we would like to emphasize that all evidence gathered so far indicates dominant antiferromagnetic interactions between the magnetic moments in all of the semimagnetic semiconductors which have been studied. According to the present understanding of spin-glasses, randomness combined with either competition or frustration seem to be essential ingredients for the existence of a spin-glass. It has been shown theoretically[30] that a diluted magnetic array on a fcc host lattice coupled by *nearest-neighbor* anitferromagnetic interactions results in a spin-glass when the concentration of magnetic ions x exceeds the percolation limit x_c. The appearance of a spin-glass phase in $Cd_{1-x}Mn_xTe$ and related SMSC's therefore could be related to these topological frustration effects in view of the fcc symmetry of the host lattice.[4]

Recently, however, it has been shown that the spin-glass transition also exists for concentrations below x_c for SMSC's such as $Cd_{1-x}Mn_xTe$, $Hg_{1-x}Mn_xTe$, etc. and extends in fact down to $x=0$, as a consequence of the long-range character of the interactions.[6,8] It seems to us that these observations of spin-glass behavior for $x<x_c$ cannot be understood on the basis of the above-mentioned theoretical predictions. The situation for $(Cd_{1-x}Mn_x)_3As_2$ is even more pronounced since in this case, for $x>x_c$, the nearest-neighbor frustration mechanism is also excluded due to the simple cubic symmetry of the host lattice.

In conclusion, we feel that the spin-glass behavior of $(Cd_{1-x}Mn_x)_3As_2$ (but also of the well-known SMSC's such as $Cd_{1-x}Mn_xTe$, $Hg_{1-x}Mn_xTe$, etc. for $x<x_c$) cannot be understood on the basis of the present ideas about the essential characteristics of the spin-glass formation.

ACKNOWLEDGMENTS

The authors wish to acknowledge numerous fruitful discussions with K. Kopinga, F. A. P. Blom, and H. M. A. Schleypen. Thanks are due to C. van der Steen and J. Millenaar for technical assistance and advice, to H. J. M. Heyligers for his help in the analysis of the samples, and to P. A. M. Nouwens for preparing the samples. We also thank T. Sakakibara, S. Takeyama, T. Goto, and N. Miura for their help in the high-field magnetization measurements.

*Permanent address: Institute for Solid State Physics, University of Tokyo, Roppongi 7, Tokyo 106, Japan.

[1]W. J. M. de Jonge, M. Otto, C. J. M. Denissen, F. A. P. Blom, C. van der Steen, and K. Kopinga, J. Magn. Magn. Mater. **31-34**, 1373 (1983).

[2]N. B. Brandt and V. V. Moshchalkov, Adv. Phys. **33**, 193 (1984).

[3]F. A. P. Blom, J. W. Cremers, J. J. Neve, and M. J. Gelten, Solid State Commun. **33**, 69 (1980); J. J. Neve, J. Kossut, C. M. van Es, and F. A. P. Blom, J. Phys. C **15**, 4795 (1982); J. J. Neve, C. J. R. Bouwens, and F. A. P. Blom, Solid State Commun. **38**, 27 (1981).

[4]R. R. Galazka, S. Nagata, and P. H. Keesom, Phys. Rev. B **22**, 3344 (1980).

[5]S. Nagata, R. R. Galazka, D. P. Mullin, H. Akbarzadeh, G. D. Khattak, J. K. Furdyna, and P. H. Keesom, Phys. Rev. B **22**, 3331 (1980).

[6]N. B. Brandt, V. V. Moshchalkov, A. O. Orlov, L. Skrbek, I. M. Tsidil'kovskii, and S. M. Chudinov, Zh. Eksp. Teor. Fiz. 84, 1050 (1983) [Sov. Phys.—JETP **57**, 614 (1983)].

[7]M. Escorne, A. Mauger, J. L. Tholence, and R. Triboulet, Phys. Rev. B **29**, 6306 (1984).

[8]M. A. Novak, O. G. Symko, D. J. Zheng, and S. Oseroff, J. Appl. Phys. **57**, 3418 (1985).

[9]M. A. Novak, O. G. Symko, D. J. Zheng, and S. Oseroff, Physica **126B**, 469 (1984).

[10]Y. Shapira, S. Foner, D. H. Ridgley, K. Dwight, and A. Wold, Phys. Rev. B **30**, 4021 (1984); R. L. Aggarwal, S. N. Jasperson, Y. Shapira, S. Foner, T. Sakakibara, T. Goto, N. Miura, K. Dwight, and A. Wold, in *Proceedings of the 17th International Conference on the Physics of Semiconductors, San Francisco (1984),* edited by J. D. Chadi and W. A. Harrison (Springer-Verlag, Berlin, 1985), p. 1419.

[11]W. Żdanowicz, K. Kloc, A. Burian, B. Rzepa, and E. Żdanowicz, Crystallogr. Res. Technol. **18**, K25 (1983).

[12]G. A. Steigmann and J. Goodyear, Acta Crystallogr. Sect. B **24**, 1062 (1968).

[13]J. Souletie, J. Phys. (Paris), Colloq. **39**, C2-3 (1978); J. L. Tholence and R Tournier, *ibid.* **35**, C4-229 (1974).

[14]M. Escorne, A. Mauger, R. Triboulet, and J. L. Tholence, Physica **107B**, 309 (1981).

[15]A. Mycielski, C. Rigaux, M. Menant, T. Dietl, and M. Otto, Solid State Commun. **50**, 257 (1984).

[16]J. A. Gaj, R. Planel, and G. Fishman, Solid State Commun. **29**, 435 (1979).

[17]K. Matho, J. Low Temp. Phys. **35**, 165 (1979); M. D. de Núñez-Reguiro, Ph.D. thesis, Université de Grenoble, 1980 (unpublished).

[18]A. F. J. Morgownik and J. A. Mydosh, Solid State Commun. **47**, 321 (1983).

[19]W. Dobrowolski, M. von Ortenberg, A. M. Sandauer, R. R. Galazka, A. Mycielski, and R. Pauthenet, *Proceedings of the Conference on the Physics of Narrow Gap Semiconductors, Linz, Austria, 1981,* edited by E. Gornik, H. Heinrich, and L. Palmetshofer (Springer-Verlag, Berlin, 1982), p. 302.

[20]M. A. Ruderman and C. Kittel, Phys. Rev. **96**, 99 (1954); K. Yosida, *ibid.* **106**, 893 (1957); T. Kasuya, Prog. Theor. Phys. **16**, 45 (1956).

[21]C. Lewiner and G. Bastard, J. Phys. C **13**, 2347 (1980); C. Lewiner, J. A. Gaj, and G. Bastard, J. Phys. (Paris) **41**, C5-289 (1980).

[22]N. Bloembergen and T. J. Rowland, Phys. Rev. **97**, 1679 (1955).

[23]B. E. Larson, K. C. Hass, H. Ehrenreich, and A. E. Carlsson, Solid State Commun. **56**, 347 (1985).

[24]J. J. Neve, Ph.D. thesis, University of Technology Eindhoven, 1984 (unpublished).

[25]R. J. Wagner, E. D. Palik, and E. M. Swiggard, Proceedings of the Conference on the Physics of Semimetals, Narrow-Gap Semiconductors, Dallas [J. Phys. Chem. Solids Suppl. 1, 471 (1970)].

[26]R. Plumier and F. K. Lotgering, Solid State Commun. **8**, 477 (1970).

[27]W. Geertsma, C. Haas, G. A. Sawatzky, and G. Vertogen, Physica **86-88A**, 1039 (1977); G. A. Sawatzky, W. Geertsma, and C. Haas, J. Magn. Magn. Mater. **3**, 37 (1976); C. E. T. Concalves da Silva and L. M. Falicov, J. Phys. C **5**, 63 (1972).

[28]D. G. Andrianov, N. M. Pavlov, A. S. Savel'ev, V. I. Fistul', and G. P. Tsiskarishvili, Fiz. Tekh. Poluprovodn. **14**, 1202 (1980) [Sov. Phys.—Semicond. **14**, 711 (1980)].

[29]P. Maheswaranathan, R. J. Sladek, and U. Debska, Phys. Rev. B **31**, 7910 (1985); A. Franciosi, C. Caprile, and R. Reifenberger, *ibid.* **31**, 8061 (1985); P. Maheswaranathan, R. J. Sladek, and U. Debska, *ibid.* **31**, 5212 (1985); P. Oelhafen, M. P. Vecchi, J. L. Freeouf, and V. L. Moruzzi, Solid State Commun. **44**, 1547 (1982); B. Orlowski, K. Kopalko, and W. Chab, *ibid.* **50**, 749 (1984).

[30]L. De Seze, J. Phys. C **10**, L353 (1977); J. Villain, Z. Phys. B **33**, 31 (1979); G. S. Grest and E. F. Gabl, Phys. Rev. Lett. **43**, 1182 (1979).